Performance of Power Limited Differential Power Processing Architectures in Mismatched PV Systems

Carlos Olalla, *Member, IEEE*, Chris Deline, *Member, IEEE*, Daniel Clement, *Student Member, IEEE*, Yoash Levron, *Member, IEEE*, Miguel Rodriguez, *Member, IEEE*, Dragan Maksimovic, *Senior Member, IEEE*

Abstract

Differential power processing (DPP) architectures employ distributed, low power processing, submodule integrated converters to mitigate mismatches in photovoltaic (PV) power systems, while introducing no insertion losses. This paper evaluates the effects of the simple voltage balancing DPP control approach on the submodule-level maximum power point (MPP) efficiency. It is shown that the submodule MPP efficiency of voltage balancing DPP converters exceeds 98% in the presence of worst-case MPP voltage variations due to irradiance or temperature mismatches. Furthermore, the effects of reduced converter power rating in the isolated-port DPP architecture are investigated by long-term, high-granularity simulations of five representative PV system scenarios. For partially shaded systems, it is shown that the isolated-port DPP architecture offers about two times larger energy yield improvements compared to full power processing (FPP) module-level converters, and that it outperforms module-level FPP approaches even when the power rating of DPP converters is only 20-30% of the PV system peak power. In the cases of aging related mismatches, more than 90% of the energy yield improvements are obtained with DPP converters rated at only 10% of the PV peak power.

The information, data, or work presented herein was funded in part by the Advanced Research Projects Agency-Energy (ARPA-E), an agency of the United States Government, U.S. Department of Energy, under Award Number DE-AR0000216. Neither the United States Government nor any agency thereof, nor any of their employees, makes any warranty, express or implied, or assumes any legal liability or responsibility for the accuracy, completeness, or usefulness of any information, apparatus, product, or process disclosed, or represents that its use would not infringe privately owned rights. Reference herein to any specific commercial product, process, or service by trade name, trademark, manufacturer, or otherwise does not necessarily constitute or imply its endorsement, recommendation, or favoring by the United States Government or any agency thereof. The views and opinions of authors expressed herein do not necessarily state or reflect those of the United States Government or any agency thereof.

The work by C. Olalla was funded in part by the Generalitat de Catalunya, Beatriu de Pinòs programme under award BP-B00047.

C. Olalla is with the Department of Electrical, Electronic, and Automatic Control Engineering, Rovira i Virgili University, Tarragona, 43007 Spain (e-mail: carlos.olalla@urv.cat).

C. Deline is with the National Renewable Energy Laboratory, Golden, CO 80401 USA (e-mail: chris.deline@nrel.gov).

D. Clement, Y. Levron, M. Rodriguez and D. Maksimovic are with the Department of Electrical, Computer, and Energy Engineering, University of Colorado, Boulder, CO 80309 USA (e-mail: maksimov@colorado.edu).

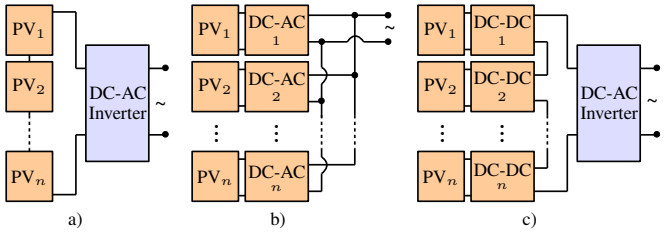

Figure 1. PV system architectures: a) conventional system with a string or central inverter, b) system with module-level DC-AC inverters or *micro*inverters, c) system with cascaded DC-DC converters or *dc optimizers* followed by a central inverter.

Index Terms

Photovoltaic Modules, Sub-Module Integrated Converters, SubMICs, DC-DC Converters, Modeling and Control of Power Electronics, Renewable Energy Systems.

I. Introduction

In photovoltaic (PV) power systems, partial shading, manufacturing tolerances, or soiling, among others, cause differences in the power generated by PV cells. This results in a dispersion between each cell maximum power point (MPP). As a result, a portion of the available power is lost either within PV cells or due to bypass diodes. The losses can be significant, especially in the conventional string or central inverter based architectures, such as the system shown in Fig. 1(a) [1], [2].

Several methods have been proposed to reduce these mismatch-related losses by employing full power processing (FPP) distributed power electronics, including microinverters (Fig. 1(b)) [3], or dc optimizers (Fig. 1(c)) [4]–[7], which perform maximum power point tracking (MPPT) at the PV module level [4], [5] or even submodule level [6], [7].

More recently, several differential power processing (DPP) architectures have been proposed [8]–[11]. These DPP architectures can be classified into two groups: PV-to-PV DPP architectures where converters interface adjacent sections of the PV string [9], [10], as shown in Fig. 2(a), and those where converters interface with a bus (PV-to-bus), which can be the PV output port [8], or an isolated port [11], as shown in Fig. 2(b). The basics of these DPP architectures are similar: converters connected across groups of cells of the same size, here referred to as *submodules*, operate to balance the current through the series connected string of submodules. The DPP architectures present several advantages with respect to FPP approaches. While FPP converters process the full power of attached modules, DPP converters only process the power difference between them. This allows the reduction of the power rating of DPP converters to a fraction of the submodule peak power, thus reducing the size and cost of power electronics. In consequence, there are more opportunities to implement DPP architectures at higher granularity, i.e. at submodule level, effectively replacing bypass diodes [11], or even at the cell level. Since cells operate closer to their individual MPP, energy capture in the presence of mismatches is improved [12], [13]. Furthermore, it is expected that DPP architectures can lead to reliability improvements related to mitigation of hot spots in PV systems

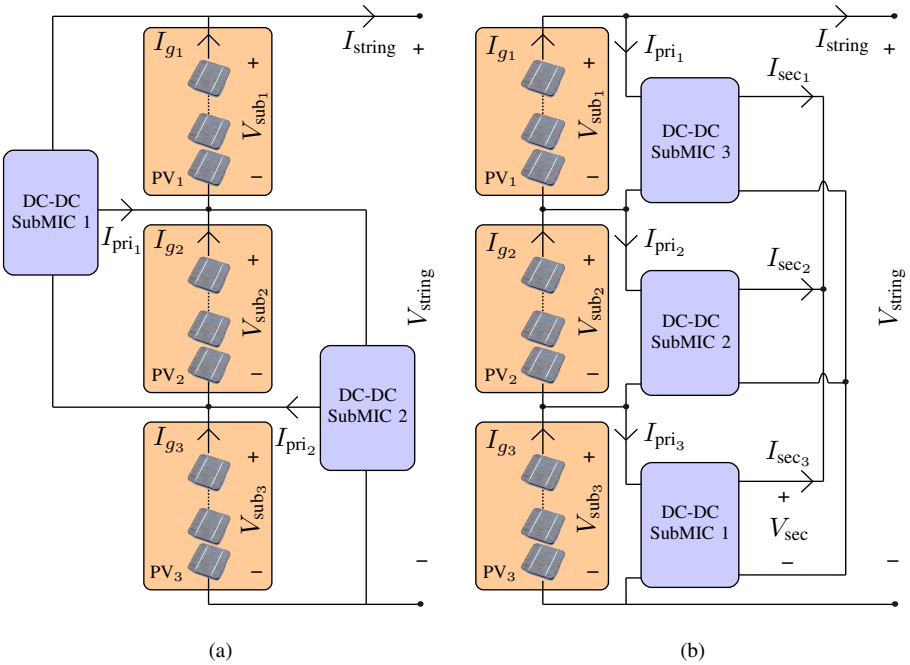

Figure 2. Differential power processing (DPP) architectures: a) PV-to-PV shuffling converters, and b) isolated-port PV-to-bus architecture.

[14], [15].

The objectives of this paper are to address the performance of DPP architectures in relation to the MPP efficiency at the submodule level, conversion efficiency of submodule level DPP converters, and their power rating relative to the PV submodule peak power rating. The paper is organized as follows. Section II defines PV system available power and efficiency for three PV system architectures: the conventional architecture of Fig. 1(a), the architecture shown in Fig. 1(c) with module-level FPP dc optimizers, i.e. module integrated converters (MICs), and the DPP architecture with submodule-integrated converters (subMICs). The performance of DPP architectures depends on the amount of mismatch in the system, the submodule-level MPP efficiency, the subMIC power conversion efficiency, and the subMIC power rating. Focusing on the case when subMICs are operated to simply balance the submodule voltages [9]–[11], Section III examines the effects of mismatch in submodule MPP voltage, the consequent MPP efficiency losses and the influence of the steady-state regulation error. In Section IV, the combined effects of submodule-level MPP efficiency, subMIC power conversion efficiency, as well as the effects of limiting subMIC power rating to a fraction of the submodule peak power, are examined for the isolated-port DPP architecture in five representative PV systems, including mismatches due to partial shading and aging effects. The results are summarized and conclusions are discussed in Section V.

II. Photovotaic power system available power and efficiency

Consider a PV power system having a string of n_{mod} PV modules in series, each module consisting of n_{sub} submodules in series, and each submodule comprising n_c series-connected PV cells. Given solar irradiation and

temperature for each of the n_{cell} cells in the string, $n_{\text{cell}} = n_{\text{mod}} \times n_{\text{sub}} \times n_c$, the *total available* system power P_{av} can be found as

$$P_{\text{av}} = \sum_{i=1}^{n_{\text{cell}}} P_{\text{mpp},i}^{\text{cell}} \,, \tag{1}$$

where $P_{\text{mpp},i}^{\text{cell}}$ is the MPP power for the i^{th} cell. From the energy capture perspective, the overall system efficiency can be defined as

$$\eta_{\text{sys}} = \frac{P_{\text{ac}}}{P_{\text{av}}} \,, \tag{2}$$

where P_{ac} is the power delivered to the grid. It is of interest to examine the factors contributing to η_{sys} in different PV system architectures. In the conventional system shown in Fig. 1(a), a string inverter operates the string of PV modules at the string MPP, and delivers P_{ac} to the grid. For a given operating point, the system efficiency can therefore be written as

$$\eta_{\text{sys,string}} = \eta_{\text{cell-string}} \times \left(\eta_{\text{mpp,string}} \times \eta_{\text{inv}}\right) , \tag{3}$$

where $\eta_{\text{mpp,string}}$ is the MPP tracking efficiency of the inverter, and η_{inv} is the inverter dc-to-ac power conversion efficiency. Factor $\eta_{\text{cell-string}}$ models the effects of mismatches among the cells in the string. If all cells are perfectly matched, $P_{\text{av}} = n_{\text{cell}} P_{\text{mpp}}^{\text{cell}}$ and $\eta_{\text{cell-string}} = 1$. In practical systems, $\eta_{\text{cell-string}}$ can be as low as $70-80\%$ in residential installations with partial shading [16]. Even in large commercial or utility-scale installations without any significant irradiance mismatches, $\eta_{\text{cell-string}}$ is often below $95-98\%$ due to temperature gradients, uneven soiling, and tolerances that increase with ageing [17]. The relatively large impact of mismatches on the energy yield has motivated research in distributed power electronics architectures. For example, in an FPP system with module-level dc optimizers, as shown in Fig. 1(c), the system efficiency can be expressed as

$$\eta_{\text{sys,FPP}} = \eta_{\text{cell-module}} \times \left(\eta_{\text{mpp,mod}} \times \eta_c\right) \times \eta_{\text{inv}} \,, \tag{4}$$

where $\eta_{\text{mpp,mod}}$ is the MPP tracking efficiency of the dc optimizer or MIC, η_c is the MIC power conversion efficiency, and factor $\eta_{\text{cell-module}}$ models the cell mismatch effects at the module level. Since $\eta_{\text{cell-module}} > \eta_{\text{cell-string}}$ [16], and because MIC conversion efficiencies can be very high, a dc optimizer system can outperform conventional systems in terms of system efficiency and energy capture [12], [16]. Note, however, that the inclusion of dc optimizers brings in an additional conversion efficiency term η_c, which represents the insertion loss of this architecture. FPP systems can perform worse than conventional approaches when the effects of mismatch are not significant ($\eta_{\text{cell-module}} \approx \eta_{\text{cell-string}}$ or $\eta_{\text{cell-submod}} \approx \eta_{\text{cell-string}}$). An example case of this possibility can be found in [18].

Consider now a DPP architecture with submodule integrated converters or subMICs. It is important to note that MPP tracking is performed at the submodule level using subMICs that process only a mismatch portion α_{sub} of power. At the PV string dc output, as in a conventional system, a string or central inverter performs MPP tracking at the string level, and delivers power to the ac grid. The system efficiency for the DPP architecture can be written as:

$$\eta_{\text{sys,DPP}} = \eta_{\text{cell-submod}} \times \left(\eta_{\text{mpp,sub}} \times \eta_{\text{sub}}\right) \times \left(\eta_{\text{mpp,string}} \times \eta_{\text{inv}}\right) , \tag{5}$$

where $\eta_{\text{mpp,sub}}$ is the MPP tracking efficiency of the DPP converters at the submodule level, and

$$\eta_{\text{sub}} = 1 - \alpha_{\text{sub}} \times (1 - \eta_c) \tag{6}$$

represents the impact of the subMIC power processing efficiency η_c. Several DPP advantages can be deduced by comparing (5) to (4) and (3): first, since power processing is performed at finer granularity, $\eta_{\text{cell-submod}} > \eta_{\text{cell-module}} > \eta_{\text{cell-string}}$ [16]; second, subMICs process only a mismatch portion of power, $\alpha_{\text{sub}} < 1$. As a result, the effect of subMIC power conversion efficiency on system efficiency is reduced. For example, assuming $\alpha_{\text{sub}} = 20\%$, the impact of a $\eta_c = 90\%$ efficient subMIC on the system efficiency is $\eta_{\text{sub}} = 98\%$. Importantly, in the case when there are no mismatches, $\alpha_{\text{sub}} = 0$, and subMICs can be shut down, presenting no insertion losses, $\eta_{\text{sub}} = 100\%$. This is in contrast to series connected FPP converters, which always process full power and result in insertion losses. Finally, it should also be noted that DPP operation results in a convex string level power characteristic with a narrow range of string-level MPP voltages [11]. This, in turn, can result in improved MPP tracking and power processing efficiency of the downstream string (or central) inverter.

Given the brief summary of PV system efficiencies, the next section focuses on the impact of distributed voltage balancing on the submodule-level MPP efficiency $\eta_{\text{mpp,sub}}$ in DPP architectures.

III. Effects of Mismatch and Control Gain in Voltage Balanced DPP Systems

Ideally, DPP converters are controlled to operate each submodule at its maximum power point. An approach to accomplishing a fine-granularity MPP control has been described for a PV-to-PV architecture in [19]. As an alternative to true submodule-level MPP tracking, subMICs can be controlled to simply balance the submodule voltages [9]–[11]. An advantage of the voltage-balancing control is that it can be implemented in a completely distributed manner, with no need for communication of sensing or control signals among the subMICs.

Relatively low sensitivity of the MPP voltage V_{mpp_i} of each submodule i with respect to operating conditions has been discussed in [10]. This provides the basis for the simple voltage-balancing control of converters in DPP architectures. However, each V_{mpp_i} does depend on several factors, including irradiance, temperature gradients, or shading uniformity, for example. The impact of these factors on the submodule-level MPP efficiency $\eta_{\text{mpp,sub}}$ in a DPP-based PV system is analyzed in Subsection III-A. A simplified model that provides an upper bound on power loss and experimental data validating the outcome are shown. The model, which applies to any DPP architecture, considers perfect voltage balancing, i.e., all submodules share the same voltage $V_{sub_i} = V_{\text{string}}/n_{\text{s}}$, where V_{string} is given by a downstream string-level MPPT system and n_{s} is the number of submodules in the string. In practice, perfect balancing may not be feasible, and a steady-state error between the voltage reference and the submodule voltage exists, depending on the effective DC gain in the control of these voltages. Subsection III-B elaborates on this aspect, considering the isolated-port subMIC architecture, showing that there exists an ideal voltage control gain, which maximizes $\eta_{\text{mpp,sub}}$.

A. *Effects of MPP Voltage Sensitivity*

As stated above, several factors impact the MPP voltage of each submodule. Typically, the MPP voltage decreases with increasing temperature and decreasing irradiance. In order to study the impact of any factor that modifies the MPP voltage of a submodule from its nominal value, the following simple model is proposed: assume that DPP converters present no conversion losses and regulate each submodule to a certain target voltage, $V_{\text{target}} = V_{\text{string}}/n_{\text{s}}$, such that the relative error can be expressed as:

$$\epsilon_i = \frac{V_{\text{mpp}_i} - V_{\text{target}}}{V_{\text{mpp}_i}}, \tag{7}$$

V_{mpp_i} being the true MPP voltage of submodule i. Defining S as the slope of the power vs. voltage curve near the target voltage:

$$S = \left.\frac{dP}{dV}\right|_{V \approx V_{\text{target}}}, \tag{8}$$

the relative power loss caused by each submodule i being regulated to V_{target} instead of V_{mpp_i} can be approximated as

$$\frac{\Delta P}{P_{\text{av}}} = 1 - \eta_{\text{mpp,sub}} \approx \frac{|S| V_{\text{mpp}^*} \sum |\epsilon_i|}{P_{\text{av}}}, \tag{9}$$

V_{mpp^*} being the highest submodule MPP voltage and P_{av} the system available power if all MPP points are tracked perfectly. If a conservative slope S is used here, the model (9) gives an upper bound on the power loss due to different V_{mpp_i} values across the PV string. The proposed model is used next to predict the power loss under the influence of the three main factors modifying the MPP voltage: irradiance mismatch, temperature gradient, and submodule irradiance uniformity. The results are validated by experiments.

1) Irradiance mismatch: Figure 3 shows experimental power vs. voltage curves measured, at the same temperature, for three 24-cell submodules, in a 72-cell (180 W) monocrystalline silicon PV module (Conergy S175MU). Each submodule is separately biased using current sources, emulating different irradiance levels. It can be observed that a 75% decrease in irradiance yields around 10% decrease in the submodule MPP voltage.

If two submodules are irradiated at 800 W/m^2 and the third one is irradiated at 200 W/m^2, then from the experimental data, V_{mpp_1} = V_{mpp_2} = 12.75 V, V_{mpp_3} = 11.83 V, and V_{target} = 12.5 V. Note that the change in V_{mpp_3} represents a reduction of approximately 7% with respect to V_{mpp_1} and V_{mpp_2}. The available power is P_{av} = 107 W and the maximum power vs. voltage slope is $|S| \leq$ 1.5 W/V. Also note that the areas of validity of the bound in $|S|$ are denoted as the hatched areas in Fig. 3. In this case, model (9) yields:

$$\frac{\Delta P}{P_{\text{av}}} \leq \frac{1.5 \ \frac{\text{W}}{\text{V}} 12.75 \ \text{V}(0.02 + 0.02 + 0.05)}{107 \ \text{W}} \leq 1.6\%. \tag{10}$$

The same conditions are reproduced in an experimental setup with 3 flyback subMIC prototypes described in [11], arranged as shown in Fig. 2(b). The measurements, which are adjusted to account for known conversion losses, indicate an output power of 106 W and thus a 0.93% loss due to different V_{mpp_i}. Thus, both experiments and calculations indicate that the impact of the irradiance mismatch on submodule-level MPP tracking is relatively small, less than 2%.

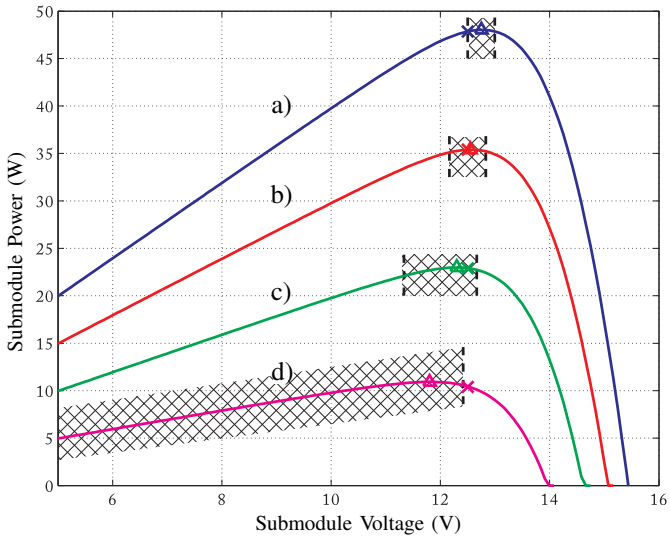

Figure 3. Experimental power-voltage characteristics for several irradiance values: a) 4 A, 800 W/m^2; b) 3 A, 600 W/m^2; c) 2 A, 400 W/m^2; d) 1 A, 200 W/m^2. $\times$ marks: target voltage, V_{target}. $\triangle$ marks: MPP voltage, V_{mpp_i}. The hatched area in each curve delimits the region where $|S| \leq 1.5$ W/V holds.

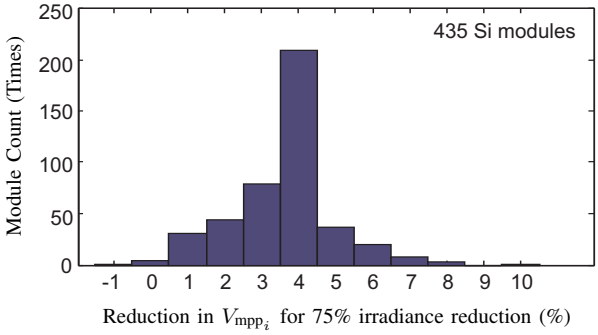

Figure 4. Survey of PV modules in the Sandia Array Performance Model database [20]. Given a reduction in irradiance from 1000 W/m^2 to 250 W/m^2, module V_{mpp_i} drops by 4% on average.

To investigate the sensitivity of V_{mpp_i} with respect to irradiance change more generally, a test of PV performance has been conducted for over 400 silicon PV modules [20]. Using experimentally derived empirical coefficients available in [21], the impact of irradiance on V_{mpp_i} is determined, assuming constant temperature. The histogram of the results given in Fig. 4 indicates that, on average, V_{mpp_i} is reduced by only 4%, given a 75% reduction in irradiance, less than the 7% reduction considered in the experiment described above. It can therefore be concluded that the effects of uniform irradiance mismatches on V_{mpp_i} are in general smaller than the particular case considered in the experiments.

As a final remark, it should be noted that thin-film modules in the database have been excluded from the analysis in Fig. 4. These modules can present high series resistances, which in extreme cases result in higher V_{mpp_i} with

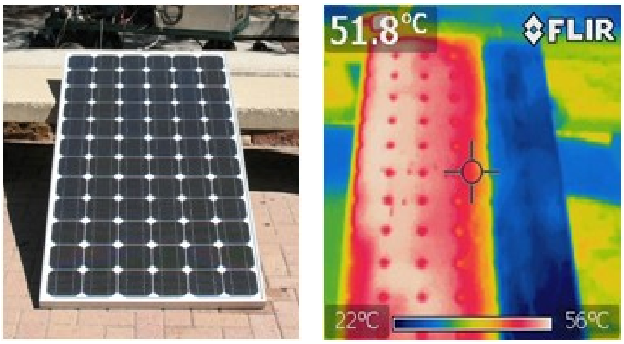

(a) (b)

Figure 5. Experimental setup used to examine PV characteristics at different temperatures. a) PV module; b) thermal image of the PV module after the temperature of one of the submodules is artificial reduced.

decreasing irradiance. Nevertheless, such a high series resistance is an undesired characteristic, and modules typically present a reduction of V_{mpp_i} with decreasing irradiance.

2) Temperature gradient: In PV systems, temperature gradients are usually caused by nonuniform irradiance. The experiments described in this section are carried out to isolate the effects of temperature variation from irradiance variation. Figure 5 shows the experimental setup used to measure the effect of temperature differences between balanced submodules. One submodule is artificially cooled to 30^o C, while the complete module is getting full sun irradiation so that the remaining two submodules are at approximately 55^oC. The power vs. voltage characteristic of each submodule is measured under these conditions, yielding a temperature coefficient for V_{mpp_i} of -0.38%/^{o}C, which is in agreement with the manufacturer data.

The measured power curves for these two different temperatures can be seen in Fig. 6. Assuming that one submodule is at 30^oC and the other two are at 55^oC, then $V_{\text{mpp}_1} = V_{\text{mpp}_2} = 9.95$ V, $V_{\text{mpp}_3} = 11$ V, and $V_{\text{target}} = 10.3$ V. The ideal available power is $P_{\text{av}} = 124$ W, and the derivative of power with respect to voltage is found to be $|S| \leq 2.4$ W/V. Power loss due to different MPP voltages arising from the 25^oC temperature difference is then:

$$\frac{\Delta P}{P_{\text{av}}} \approx \frac{2.4\ \frac{\text{W}}{\text{V}} 11\ \text{V}(0.06 + 0.03 + 0.03)}{124\ \text{W}} \approx 2.4\%. \tag{11}$$

Experimental data with the flyback subMIC prototypes [11] exhibit an output power of 121.9 W, yielding $\Delta P/P_{\text{av}} = 1.7\%$. Such a power loss can be considered relatively small given the large 25^oC temperature difference. Furthermore, it should also be noted that the two opposing effects of reduced irradiance and reduced temperature tend to be coupled: to some extent, these two effects would cancel out the variation of the MPP voltage, since lower temperature increases V_{mpp_i} while lower irradiance reduces it. Therefore, in practical PV systems, the effective power loss under these circumstances would typically be even smaller.

3) Submodule Irradiance Uniformity: The shape of the power-voltage characteristic of each submodule also changes with nonuniform shading. Figure 7 shows experimental measurements from two submodules: one with uniform irradiance (450 W/m^2) and another one with a single cell heavily shaded by 75% to irradiance of 100 W/m^2.

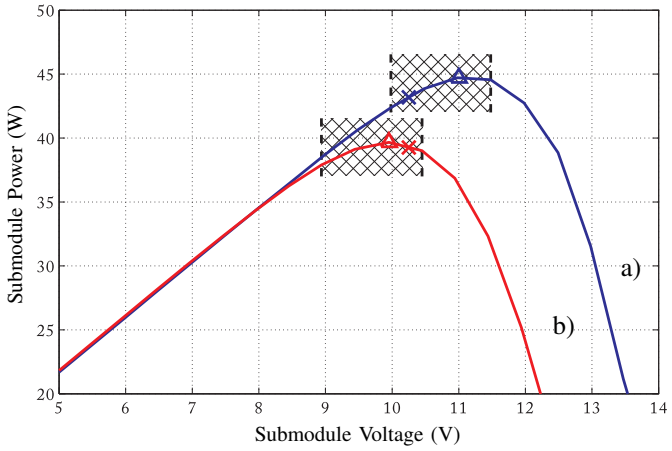

Figure 6. Experimental power-voltage characteristic against temperature: a) 30^oC, 800 W/m^2; b) 55^oC, 800 W/m^2. $\times$ marks: Target voltage, V_{target}. $\triangle$ marks: MPP voltage, V_{mpp_i}. The hatched area in each curve delimits the region where $|S| \leq$ 2.4 W/V holds.

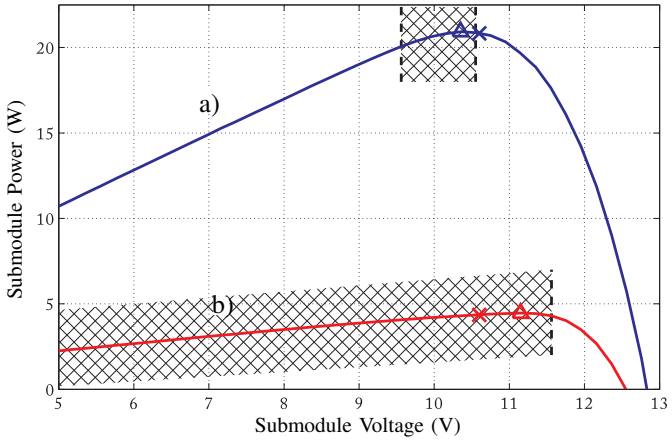

Figure 7. Experimental power-voltage characteristic against mismatch uniformity: a) uniform irradiance, 450 W/m^2; b) single-cell shaded to 100 W/m^2. $\times$ marks: Target voltage, V_{target}. $\triangle$ marks: MPP voltage, V_{mpp_i}. The hatched area in each curve delimits the region where $|S| \leq$ 1.6 W/V holds.

It can be observed that this heavy, isolated shading not only reduces the maximum available power, but also modifies the shape of the power-voltage curve of the non-uniformly shaded submodule. As a consequence, the MPP voltage of the submodule increases by around 25%. From the experimental data, V_{target} = 10.6 V, $V_{\text{mpp}_1} = V_{\text{mpp}_2}$ = 10.35 V, V_{mpp_3} = 11.15 V, $S \leq$ 1.6 W/V, P_{av} = 105.6 W. Substitution of these values into (9) yields:

$$\frac{\Delta P}{P_{\text{av}}} \approx \frac{11.15 \text{ V} \, (0.02 + 0.02 + 0.05) \, 1.6 \, \frac{\text{W}}{\text{V}}}{105.6 \text{ W}} \approx 1.5\%. \tag{12}$$

Experimental data with the flyback subMIC prototypes [11] resulted in an output power of 104.9 W, yielding $\Delta P / P_{\text{av}}$ = 0.9%. Again, the impact of the variation of the power-voltage characteristic on the voltage balance of PV submodules is less than 1%.

In summary, the effect of MPP variation for the different mismatch sources shown here can be considered small,

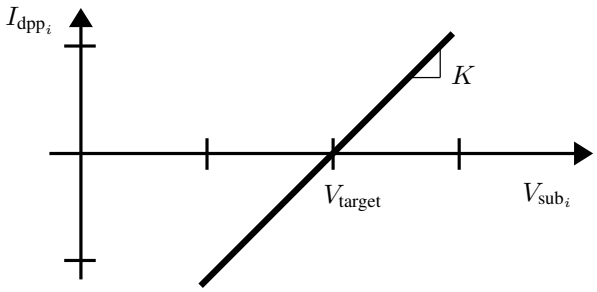

Figure 8. Linear control of DPP converter current with DC gain K.

in the case when each submodule voltage tracks the target voltage perfectly, i.e. the case when submodule voltages are perfectly balanced. A finite-gain controller results in differences between submodule voltages and the target voltages. The next section demonstrates that an optimal DC gain of the controller can be found that results in the submodule voltages closer to the true MPP values, thus further increasing $\eta_{\text{mpp,sub}}$.

B. Effects of Voltage Balancing Controller Gain

In order to achieve voltage balancing, DPP converters inject or subtract a current I_{dpp_i} from submodules depending on the error between the target voltage and each submodule individual voltage:

$$I_{\text{dpp}_i} = f_{\text{dpp}}(V_{\text{sub}_i} - V_{\text{target}}). \tag{13}$$

Several voltage balancing controllers f_{dpp} have been reported. In [11] a linear f_{dpp} is described. Other current-voltage characteristics may simplify controller implementation, such as the controllers described in [9], [22], which employ the converter duty-cycle as the control input. In [22], the current-voltage error function is nonlinear, while the DC gain of the voltage control is ideally infinite in [9], and its effective value depends on the power loss of the DC-DC converters.

In the isolated-port subMIC architecture of [11], a linear controller is employed, such that (13) can be rewritten in steady-state as:

$$I_{\text{dpp}_i} = K(V_{\text{sub}_i} - V_{\text{target}}). \tag{14}$$

The current-voltage characteristic of subMICs can then be easily described, as depicted in Fig. 8. Given that the difference between submodule voltages and the target voltage is proportional to subMIC currents, each particular PV system can easily be analyzed to determine an optimal gain K which maximizes the power output. Note, however, that K must be positive for the correct balancing of subMICs, hence this approach can only improve the efficiency in the typical case of decreasing values of V_{mpp_i} with decreasing MPP current, as shown in the previous subsection.

As an example, Fig. 9 shows the current-voltage characteristics of the three submodules in the 180 W module used above, under mismatched conditions. The module V_{mpp} is approximately 37.5 V, hence V_{target} = 12.5 V. The figure shows that the equilibrium voltages of submodules (○ marks) depend on the controller gain. When the gain

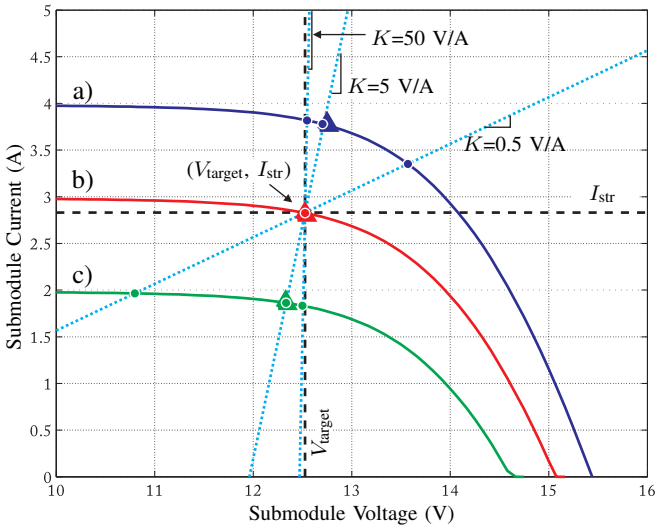

Figure 9. Linear control of DPP converter current with DC gain K for different irradiance levels. ∘ marks: operating points for the different DC gains. △ marks: MPP voltage

is K=50 V/A, the submodule voltages are very close to the target voltage and relatively close to the MPP voltages (△ marks); if the gain K equals 5 V/A, the submodule voltages do not track V_{target} perfectly, but very closely match the MPP values; finally, a low gain value of K=0.5 V/A results in poor voltage balancing and submodule voltages are far from the MPP and target voltages.

Thanks to the linear voltage-current characteristic of the controller, for any V_{target} set by the external MPPT system, the distance from each submodule current I_{g_i} to the string current I_{str} is proportional to the distance from V_{sub_i} to V_{target}:

$$\frac{(n_{\text{s}}-1)\,I_{g_i}-\sum_{\substack{j=1\\ j\neq i}}^{n_{\text{s}}} I_{g_j}}{(n_{\text{s}}-1)\,V_{\text{sub}_i}-\sum_{\substack{j=1\\ j\neq i}}^{n_{\text{s}}} V_{\text{sub}_j}} = K, \quad \forall i = 1,\ldots,n_{\text{s}}. \tag{15}$$

As a consequence, the optimal value of this linear gain K can be selected by considering the current-voltage characteristic of the specific PV system. Assuming that temperature gradients can be neglected across the system, and that the mismatch distribution is approximately uniform across submodules, a possible solution is to compute the slope of a weighted best-fit line between the MPPs for different irradiance levels. One may further note that a choice of K amounts to shaping the loadline characteristic of the converter at the primary port.

Figure 10 shows the MPPT efficiency $\eta_{\text{mpp,sub}}$ depending on the value of K, for the example of Fig. 9, neglecting conversion losses. It can be observed that a minimum gain should be chosen in order to avoid poor regulation, but high values of K also achieve high efficiency without significant degradation of performance.

This result is particularly important for other control approaches, such as the simple, nonlinear controller of [22]. Such a controller does not satisfy the proportional relationship of (15), and the effective gain increases with the difference between submodule voltages. In [22], it is shown that the maximum difference between two submodule

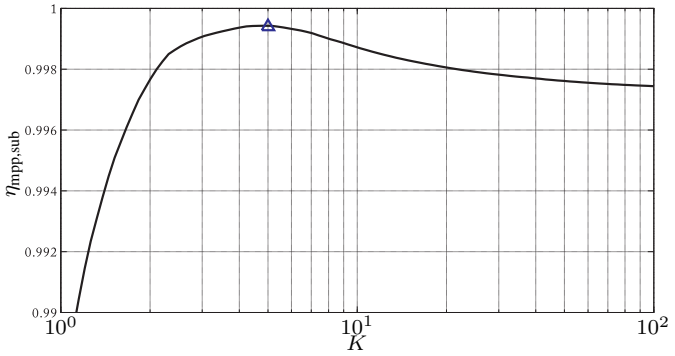

Figure 10. Submodule-level MPP efficiency ($\eta_{\text{mpp,sub}}$) for increasing values of K for the example shown in Fig. 9. It can be observed that the optimal ($\triangle$ mark) is located approximately at K=5 A/V.

voltages is bounded by some constant C and the controller gain K_p as:

$$|V_{\text{sub}_i} - V_{\text{sub}_j}| \leq \frac{C}{K_p}, \quad \forall i, j = 1, \ldots, n_{\text{s}}, i \neq j. \tag{16}$$

Since this bound holds for any submodule current difference, a minimum effective gain can be imposed using this formula, while higher effective gains are not a concern because they do not degrade performance significantly.

IV. Effects of SubMIC Power Processing Limits

The results of the previous section assume that DPP converters are rated at sufficiently high power, such that they can balance the submodules in the PV system string even under 100% mismatch. In the isolated-port DPP architecture [11], the worst case maximum required subMIC power P_{max} equals $P_{\text{max}} = P_{\text{mpp}}(n_{\text{s}} - 1)/n_{\text{s}}$, which means that subMICs can be rated below 100%. Furthermore, such extreme mismatch conditions occur very rarely or never. It is therefore of interest to investigate the effects of limiting the converter power rating to a fraction of the PV submodule peak power, in order to reduce the size and cost. The results in [23] indicate that the processed power ratio is likely to be the lowest in the PV-to-bus architectures, and this section is focused on the isolated-port PV-to-bus architecture.

SubMICs with power limits below the bound required to support the extreme 100% mismatch may not be able to process the current required in order to balance the mismatched submodules. In such case, the main problem is that the distances between MPP and submodule voltages and currents are no longer known. Shifts of the error and even of the target voltages may occur. Effects in long term energy performance are *a priori* unpredictable. In order to evaluate the impact of this limitation, long time-span and Monte Carlo simulations of representative PV systems have been carried out and are described in this section. The simulation scenarios are the same as the scenarios reported in [13]: 3 cases of PV systems affected by partial shading, and 2 cases of PV systems affected by aging:

- Scenario I: A large utility-scale system affected by partial shading.
- Scenario II: A residential system shaded by nearby trees.
- Scenario III: A residential system shaded by a chimney.

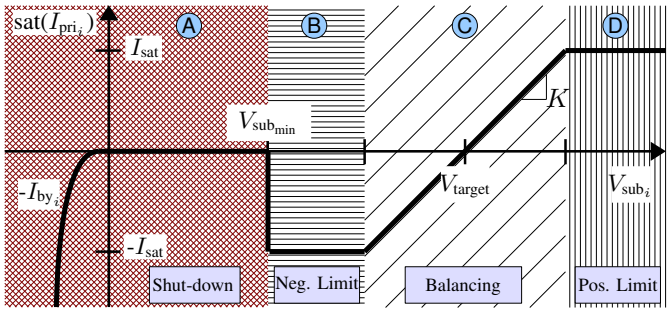

Figure 11. Nonlinear function of subMIC primary currents with respect to subMIC primary-port voltages: A) shut-down and bypass region; B) negative saturation; C) linear balancing control; D) positive saturation.

Figure 12. Scenario I: utility-scale system. Top image shows detail of partial shading from nearby light poles.

- Scenario IV: An aging mismatch simulation applied to the utility-scale system in Scenario I.
- Scenario V: An aging mismatch simulation applied to the residential system of Scenario II.

As in [13], system-level MPPT with a central inverter is considered the *conventional* operation. Previous data on string-level inverters can be found in [12], thus this case has not been considered here. Whenever module and submodule-level dc optimizer simulations are shown, FPP converters are considered to have η_c = 97.5% conversion efficiency, corresponding to the measured weighted efficiency for a commercial DC-DC converter device [24]. Note that this can yield optimistic results, especially in the case of FPP submodule converters, where it may be difficult to achieve high efficiencies at low power levels. For DPP subMIC simulations, the devices are either assumed to have ideal η_c = 100%, or to be *nonideal* subMICs with a conversion efficiency of η_c = 90%, such as the experimental prototypes described in [11]. Furthermore, nonideal 90% efficient subMICs can be rated at full power (100% of the submodule peak power rating P_{mpp}), or at a fraction of the submodule peak power. In the system efficiency comparisons, the string inverter efficiencies are disregarded, i.e., it is assumed that η_{inv} = 100%, and that $\eta_{\text{mpp,string}}$ = $\eta_{\text{mpp,mod}}$ = 100%. Further improvements that the DPP architecture offers in η_{inv} by presenting a narrow range of MPP voltages at the inverter input are not taken into account.

A. Cell Level Simulation Tool

The simulations shown in this section have been carried out by employing the cell-level tool presented in [25]. This tool adopts a cell-level model which can be solved very efficiently using standard numerical methods, and it is therefore well suited for predicting the energy capture of large PV systems over long periods of time. Descriptions of the models for partial shading and aging mismatch can be found in [13] and [25], where the tool was used to demonstrate performance improvements by DPP approaches compared to FPP approaches, but the effects of subMIC power limits have not been investigated.

In this section, the effects of power limits are taken into account as follows. SubMIC primary and secondary voltages are unrelated to the number of submodules in series n_{s}, hence devices with low voltage rating can be used. As a consequence, the current handling capabilities of the subMICs are the main limitation when reduced power rating is considered. Figure 11 shows how the submodule voltage-to-current function, shown previously in Fig. 8, becomes highly nonlinear when the maximum current that subMICs can handle is limited to I_{sat}. In the figure, $V_{\mathrm{sub_{min}}}$ stands for the minimum primary port voltage required for the subMICs to remain active, colorred given that they are powered by the primary side. If the primary voltage is lower than $V_{\mathrm{sub_{min}}}$, the subMIC shuts down and acts as a bypass diode, i.e., for negative voltages V_{sub_i}, it transfers a current -I_{by_i} as defined in [25]. The model of [25] was updated to consider these hard nonlinearities while keeping numerical efficiency, by following a branch and bound method described and experimentally verified in [26].

B. Scenario I: Partial Shading in a Utility-Scale System

The first scenario, shown in Fig. 12, considers an existing utility-scale system (8 MW) that consists of strings of 16 modules. Each module includes 3 20-cell submodules in series, with a submodule peak power rated at 81 W. Lighting poles cause partial shading on some strings, one of which being the subject of analysis in this subsection. Because of the large parallel configuration of strings, MPP voltage at the central inverter remains unchanged, leading to a daily mismatch loss of approximately 11% with respect to unshaded cases.

Table I shows the energy improvement obtained by FPP and DPP approaches in one day of operation. The ideal available energy E_{av} is the energy obtained assuming ideal cell-level MPP tracking, as noted in Section II. The recoverable mismatch-related energy loss is $(E_{\mathrm{av}} - E_{\mathrm{ac}})/E_{\mathrm{av}} \approx 11\%$, where E_{ac} is the conventional energy system output. The conventional system efficiency, neglecting any string inverter losses, is $\eta_{\mathrm{sys,string}}$ = 89.0%. While the module-level FPP architecture can improve the energy yield by 4%, the energy yield offered by the isolated-port PV-to-bus DPP architecture is more than two times higher and closer to the ideal recoverable: 9.1% for ideal subMICs, and 8.2% for nonideal $\eta_c = 90\%$ efficient subMICs. A histogram of the currents being processed by nonideal subMICs is shown in Fig. 13, where it can be noted that subMICs process low current most of the time. It is important to note, however, that in a typical mismatch situation, if one submodule is shaded, it may require a large amount of current to be balanced. While that large current is shared by the remaining subMICs, the full amount of the current injected to the shaded submodule must be processed by the corresponding subMIC. Nevertheless, excellent behavior of the DPP architecture under the effects of current limiting can be seen in Fig. 14

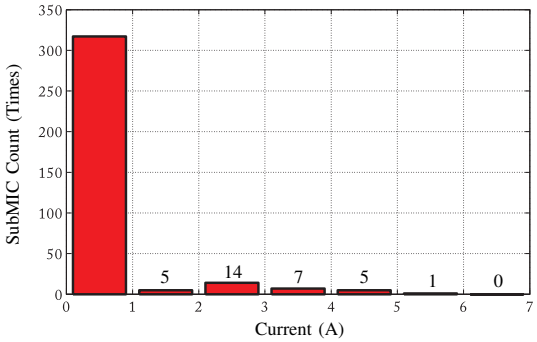

Figure 13. Scenario I: histogram of absolute value of current processed by subMICs throughout one day of simulation.

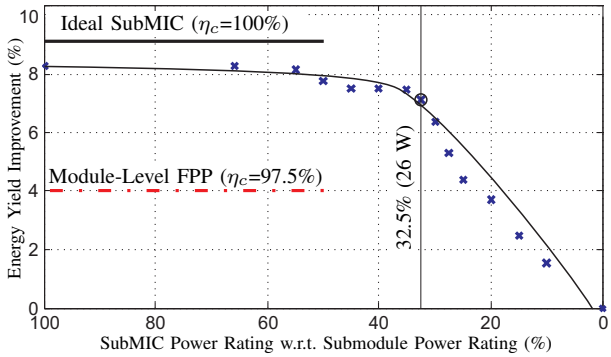

Figure 14. Scenario I: daily energy yield improvement with power limited subMICs (η_c = 90%) with respect to conventional operation. × marks: Simulation results. Solid line: Fit. 99% of the energy yield with fully rated subMICs can be achieved with subMICs rated at 32.5% (26 W) of the submodule peak power.

where the energy yield improvement relative to the conventional approach is plotted as a function of subMIC power rating normalized to the submodule peak power. Despite the large number of submodules in the string (48) and the concentration of shading on just a few of them, it can be seen that for a subMIC power rating greater than 55% of submodule peak power, daily energy yield is reduced by only 0.1%, compared to subMICs with full power rating. At the corner of the fitting line, subMICs rated at less than one third of the peak power (32.5%, 26 W) produce more than 99% of the daily energy production that would be obtained with fully rated subMICs, and result in much improved $\eta_{\text{sys,DPP}}$ = 95.5% system efficiency. Finally, the result in Fig. 14 shows that the DPP approach outperforms module-level FPP converters as long as the DPP subMIC power rating is greater than about 20% of the submodule peak power.

C. Scenario II: Residential System with Tree Shading

The second installation is a residential system for which experimental measurements have been collected since 2011. The system, rated at 2.9 kW, consists of 2 series strings of 7 modules. Each module, rated at 210 W peak power, consists of 3 36-cell submodules rated at 70 W peak power. Figure 15 gives an indication of the system

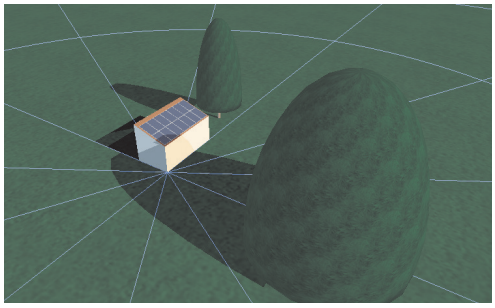

Figure 15. Scenario II: conditions in a residential PV system with shading caused by nearby trees. Annual shading calculated by ray-tracing simulation.

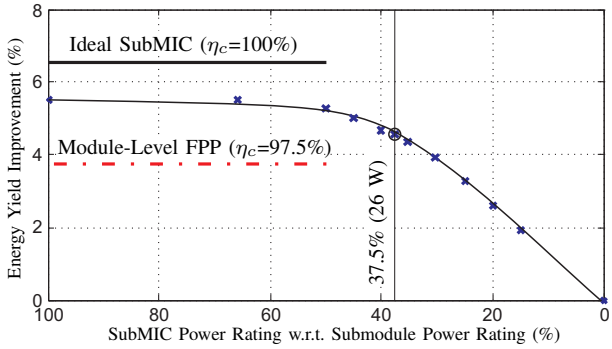

Figure 16. Scenario II: annual energy yield improvement with nonideal power limited subMICs (η_c = 90%) with respect to conventional operation. $\times$ marks: Simulation results. Solid line: Fit. 99% of the energy yield with fully rated subMICs can be achieved with subMICs rated at 37.5% (26 W) of the submodule power.

configuration, along with nearby trees, mostly providing shade in the morning and in winter. In contrast to Scenario I, shading affects a large fraction of the array, resulting in an estimated annual irradiance loss of about 20%.

The performance of the FPP and DPP approaches during one year of operation is summarized in Table II. In comparison with Scenario I, here a larger area is affected by shading, and the energy loss due to shading is about 20%, while 11% loss is recoverable. The DPP architecture outperforms module-level approaches by close to 50%, and achieves energy improvements of 6.5% and 5.5% in the ideal and nonideal cases, respectively. The yearly energy yield improvement as a function of subMIC power rating is shown in Fig. 16. The curve exhibits a flat characteristic for power ratings above 40%, and the fitting curve presents a corner at about 37.5% (26 W) where subMICs have annual energy production within 1% of fully rated subMICs. The DPP approach with subMICs rated at about 30% or above outperforms the FPP approach.

The differences between limited and unlimited power processing can be further inspected in the histogram of Fig. 17. Despite the significant reduction of 62.5% in the current handling capability of subMICs, the benefits of this DPP architecture are reduced by only 19%.

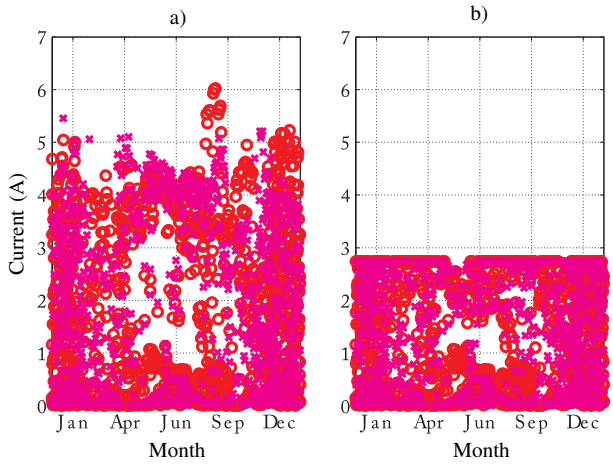

Figure 17. Scenario II: histograms of the absolute value of primary current processed by subMICs throughout one year of simulation (o: Top string, x: Bottom string): (a) conversion efficiency η_c = 90% and no current limit. (b) conversion efficiency η_c = 90% and current limit I_{sat} = 2.76 A corresponding to 37.5% of the submodule power.

Table I

SCENARIO I: ENERGY IMPROVEMENT SIMULATION RESULTS. DAILY IDEAL RECOVERABLE ENERGY: E_{av} = 19731 Wh
DAILY PRODUCTION WITH CONVENTIONAL SYSTEM LEVEL MPPT: E_{ac} = 17563 Wh, $\eta_{\text{sys,string}}$ = 89.0%

	Daily Improvement ΔE_{ac_i} (Wh)	$\Delta E_{\text{ac}_i}/E_{\text{ac}}$ (%)	Efficiency (%)
Module-Level FPP ($\eta_c = 97.5\%$)	ΔE_{ac_1}= 705 Wh	4.01%	$\eta_{\text{sys,FPP}}$ = 92.6%
Submodule-Level FPP ($\eta_c = 97.5\%$)	ΔE_{ac_2}= 1236 Wh	7.04%	$\eta_{\text{sys,FPP}}$ = 95.3%
SubMIC DPP ($\eta_c = 100\%$)	ΔE_{ac_3}= 1604 Wh	9.13%	$\eta_{\text{sys,DPP}}$ = 97.1%
SubMIC DPP ($\eta_c = 90\%$, P_{max} = 100% P_{mpp})	ΔE_{ac_4}= 1449 Wh	8.25%	$\eta_{\text{sys,DPP}}$ = 96.4%
SubMIC DPP ($\eta_c = 90\%$, P_{max} = 32.5% P_{mpp})	ΔE_{ac_5}= 1282 Wh	7.30%	$\eta_{\text{sys,DPP}}$ = 95.5%

Table II

SCENARIO II: ENERGY IMPROVEMENT SIMULATION RESULTS. YEARLY IDEAL RECOVERABLE ENERGY: E_{av} = 4536 kWh
YEARLY PRODUCTION WITH CONVENTIONAL SYSTEM LEVEL MPPT: E_{ac} = 4041 kWh, $\eta_{\text{sys,string}}$ = 89.0%

	Yearly Improvement ΔE_{ac_i} (kWh)	$\Delta E_{\text{ac}_i}/E_{\text{ac}}$ (%)	Efficiency (%)
Module-Level FPP ($\eta_c = 97.5\%$)	ΔE_{ac_1}= 152 kWh	3.76%	$\eta_{\text{sys,FPP}}$ = 92.4%
Submodule-Level FPP ($\eta_c = 97.5\%$)	ΔE_{ac_2}= 192 kWh	4.75%	$\eta_{\text{sys,FPP}}$ = 93.3%
SubMIC DPP ($\eta_c = 100\%$)	ΔE_{ac_3}= 264 kWh	6.53%	$\eta_{\text{sys,DPP}}$ = 94.9%
SubMIC DPP ($\eta_c = 90\%$, P_{max} = 100% P_{mpp})	ΔE_{ac_4}= 223 kWh	5.52%	$\eta_{\text{sys,DPP}}$ = 94.0%
SubMIC DPP ($\eta_c = 90\%$, P_{max} = 37.5% P_{mpp})	ΔE_{ac_5}= 180 kWh	4.45%	$\eta_{\text{sys,DPP}}$ = 93.1%

D. Scenario III: Residential System with Chimney Shading

A residential installation affected by a rooftop chimney shade has been considered as the third scenario. This system is similar to the one considered in [27]. It consists of 2 strings of 4 modules rated at 210 W, each module

Table III

SCENARIO III: ENERGY IMPROVEMENT SIMULATION RESULTS. YEARLY IDEAL RECOVERABLE ENERGY: E_{av} = 2872 kWh

YEARLY PRODUCTION WITH CONVENTIONAL SYSTEM LEVEL MPPT: E_{ac} = 2576 kWh, $\eta_{\text{sys,string}}$ = 89.7%

	Yearly Improvement ΔE_{ac_i} (kWh)	$\Delta E_{\text{ac}_i}/E_{\text{ac}}$ (%)	Efficiency (%)
Module-Level FPP ($\eta_c = 97.5\%$)	ΔE_{ac_1}= 53 kWh	2.17%	$\eta_{\text{sys,FPP}}$ = 91.5%
Submodule-Level FPP ($\eta_c = 97.5\%$)	ΔE_{ac_2}= 93 kWh	3.61%	$\eta_{\text{sys,FPP}}$ = 92.9%
SubMIC DPP ($\eta_c = 100\%$)	ΔE_{ac_2}= 143 kWh	5.55%	$\eta_{\text{sys,DPP}}$ = 94.7%
SubMIC DPP ($\eta_c = 90\%$, P_{max} = 100% P_{mpp})	ΔE_{ac_3}= 118 kWh	4.58%	$\eta_{\text{sys,DPP}}$ = 93.8%
SubMIC DPP ($\eta_c = 90\%$, P_{max} = 40% P_{mpp})	ΔE_{ac_4}= 89 kWh	3.45%	$\eta_{\text{sys,DPP}}$ = 92.8%

having 3 submodules rated at 70 W peak power each. Shading only affects the array during the winter months with essentially no shading-induced mismatch during summer, resulting in yearly energy loss of approximately 13%. Given the orientation of the array and the chimney, the top string is less shaded than the bottom string.

Simulation results given in Table III indicate that the annual performance improvement of DMPPT approaches is relatively small. This can be attributed to the absence of mismatch during the summer months, when energy production is larger. Indeed this aspect limits the improvement of FPP approaches, given that they process the full power of the modules during these mismatch-free periods.

In contrast, ideal subMICs would be able to recover approximately three times the energy recovered by module-level dc optimizers, producing an improvement of 5.6%. Nonideal subMICs rated at full power would perform slightly worse, improving the energy yield by 4.6%. Their annual improvement, which is shown in Fig. 19, exhibits a low dependence on the converter power processing limit for ratings above 50% of the submodule peak power. As in the previous cases, nonideal subMICs rated at 40% of the submodule peak power would allow annual energy yield within 1% of the energy produced with fully rated converters. The histogram of Fig. 20, which shows the current processed by subMICs rated at 100% and 40% of P_{mpp}, illustrates that this last result is achieved despite the fact that the processed current is reduced by more than a factor of 2 in some cases. One may also note that subMICs process no power during summer months.

E. Scenario IV: Ageing Mismatch in Utility-Scale System

In order to evaluate the energy loss due to aging effects and the possible gains with power limited subMICs, Monte Carlo simulations have been carried out for Scenarios IV and V. These two PV systems have the same configuration shown in Scenarios I and II, respectively, but they only consider mismatch derived from aging.

For the Monte Carlo simulations, random values of I_{sc} and I_{mpp} are chosen for each submodule of the installation from a normal distribution ranging from $\sigma/\mu = 1\%$ to $\sigma/\mu = 10\%$, σ being the standard deviation and μ the mean. This coefficient of variation matches the aging of a PV module over its lifetime [28], hence the expected value at submodule-level can be considered equal or higher. Note that I_{sc} and I_{mpp} are considered constant across each submodule, i.e. all cells are equal in a particular submodule. A total of 1250 cases have been evaluated for the

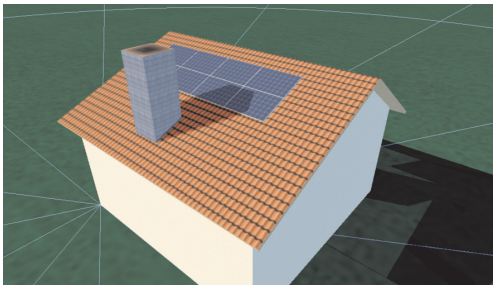

Figure 18. Scenario III: example shading conditions assumed for the residential chimney shading.

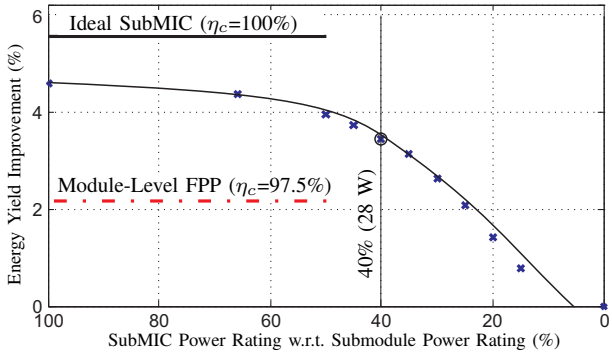

Figure 19. Scenario III: Annual energy yield improvement with power limited subMICs (η_c = 90%) with respect to conventional operation. $\times$ marks: Simulation results. Solid line: Fit. 99% of the energy yield with 100% power rated subMICs can be achieved with subMICs rated at 40% of the submodule power (28 W).

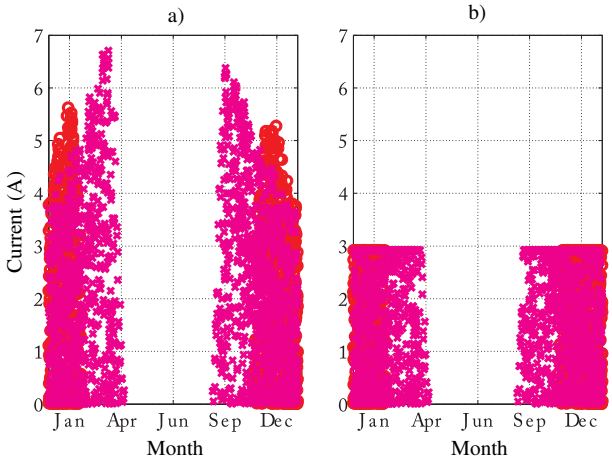

Figure 20. Scenario III: histograms of the absolute value of primary current processed by subMICs throughout one year of simulation (o: Top string, x: Bottom string): (a) Efficiency η_c = 90% and no current limit. (b) Efficiency η_c = 90% and current limit I_{sat} = 2.9 A corresponding to 40% of the submodule peak power.

conventional system, and for the DPP architecture with nonideal 90% efficient subMICs rated at 100%, 20%, 10% or 5% of the submodule peak power.

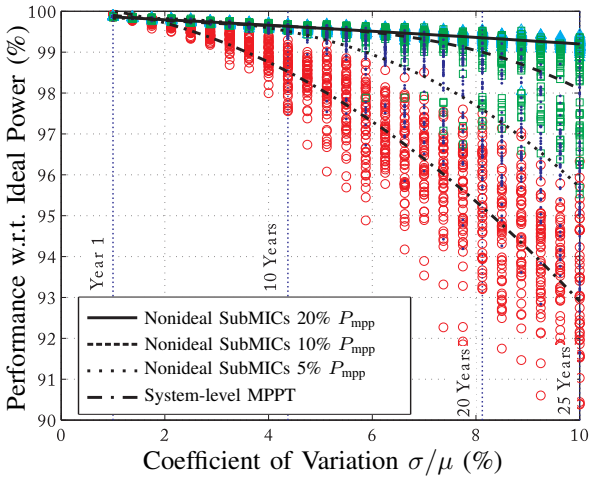

Figure 21. Scenario V: Performance (ratio between actual and ideal power) for a coefficient of variation between 1% and 10%. Conventional system-level MPPT (circles) and its best-fit curve (dash-dotted line). Nonideal subMICs rated at 5% (dots) and its best-fit curve (dotted line). Nonideal subMICs rated at 10% (squares) and its best-fit curve (dashed line). Nonideal SubMICs rated at 20% (triangles) and its best-fit curve (solid line).

The results of this simulation, considering the large utility scale string of Scenario I, are depicted in Fig. 21. Fitting lines describing the average behavior of the PV system are used to estimate the average energy yield loss over time. Table IV shows that, due to aging mismatch, there is an annual loss of 4.5% after 20 years and 7% after 25 years, when a conventional system level inverter is used. Most of this energy can be recovered, since it is lost only because of the different MPP currents in each submodule. Nonideal DPP subMICs rated at only 20% power allow the loss to be reduced to less than 0.6% annually after 20 years and to less than 0.8% after 25 years. The energy yield is improved by a lifetime total of 2.3%, which is the same as the yield obtained by fully rated subMICs.

Mitigation of aging effects is reduced if DPP subMICs are rated at less than 20%. Nevertheless, 2.1%, or more than 90% of the energy yield improvement, is obtained with subMICs rated at just 10% of the submodule peak power. Since mismatch power levels are low, the 10% rated converters behave as fully rated converters up until the coefficient of variation becomes larger than 6%, in year 15. Even lower power rating of 5% still results in lifetime energy improvement by 1.4%.

F. Scenario V: Aging Mismatch in Residential System

A similar Monte Carlo simulation has been carried out for the residential system of Scenario II. The results of this simulation, summarized in Fig. 22 and Table V, predict a mismatch loss of 5.5% after 20 years and 8% after 25 years in the conventional system. Despite having fewer modules in series, this system has more PV cells per submodule, hence the more adverse effects of mismatch. DPP subMICs allow the loss to be reduced to 0.8% after 20 years and 1% after 25 years. The simulation also provides the average energy gains thanks to subMICs: a 2.9% energy improvement can be achieved with subMICs rated at just 20% of the submodule peak power, and almost

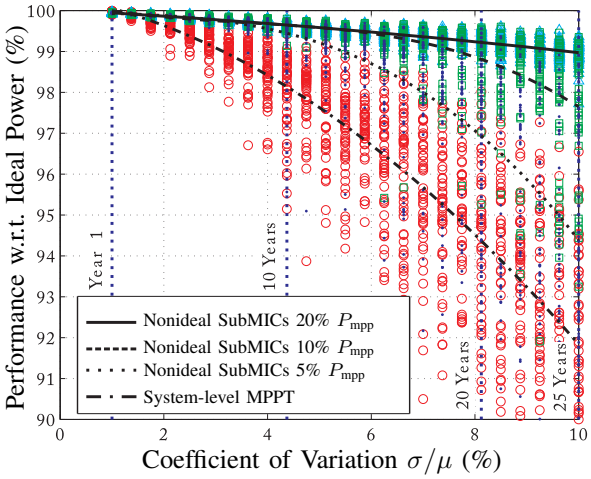

Figure 22. Scenario V: Performance (ratio between actual and ideal power) for a coefficient of variation between 1% and 10%. Conventional system-level MPPT (circles) and its best-fit curve (dash-dotted line). Nonideal subMICs rated at 5% (dots) and its best-fit curve (dotted line). Nonideal subMICs rated at 10% (squares) and its best-fit curve (dashed line). Nonideal subMICs rated at 20% (triangles) and its best-fit curve (solid line).

Table IV

SCENARIO IV: SIMULATION RESULTS

		End of Lifetime Yearly Loss (%)	Average Yearly Loss (%)	Lifetime Energy Improvement (%)
System-Level MPPT		7.10%	2.74%	-
SubMIC DPP ($\eta_c = 90\%$)	P_{max} = 100% P_{mpp}	0.80%	0.46%	2.35%
	P_{max} = 20% P_{mpp}	0.80%	0.46%	2.35%
	P_{max} = 10% P_{mpp}	1.90%	0.66%	2.14%
	P_{max} = 5% P_{mpp}	4.30%	1.35%	1.43%

Table V

SCENARIO V: SIMULATION RESULTS

		End of Lifetime Yearly Loss (%)	Average Yearly Loss (%)	Lifetime Energy Improvement (%)
System-Level MPPT		8.17%	3.26%	-
SubMIC DPP ($\eta_c = 90\%$)	P_{max} = 100% P_{mpp}	1.03%	0.50%	2.86%
	P_{max} = 20% P_{mpp}	1.03%	0.50%	2.86%
	P_{max} = 10% P_{mpp}	2.35%	0.73%	2.61%
	P_{max} = 5% P_{mpp}	5.62%	1.68%	1.64%

the same gain is obtained with 10% power rated subMICs: 2.6%. SubMICs rated at just 5% power still yield a 1.64% improvement.

Table VI
SUMMARY OF RESULTS

	Conventional System Power Loss	Energy Improvement with nonideal subMICs (η_c = 90%)	Energy Improvement with nonideal power limited subMICs (η_c = 90%)
Scenario I: Light Poles	10.92%	8.25%	7.30% (32.5% $P_{\text{mpp}} = 26W$)
Scenario II: Tree Shading	22.30%	5.52%	4.45% (37.5% $P_{\text{mpp}} = 26W$)
Scenario III: Chimney Shading	13.21%	4.58%	3.45% (40% $P_{\text{mpp}} = 28W$)
Scenario IV: Utility-Scale Ageing	2.61%	2.35%	2.35% (20% $P_{\text{mpp}} = 16W$)
Scenario V: Residential-System Ageing	3.17%	2.86%	2.86% (20% $P_{\text{mpp}} = 14W$)

V. SUMMARY OF RESULTS AND CONCLUSIONS

Differential power processing (DPP) architectures employ distributed, low power processing, submodule integrated converters to mitigate mismatches in photovoltaic (PV) power systems, while introducing no insertion losses. The DPP architectures present several advantages with respect to full power processing (FPP) approaches, such as dc optimizers. While FPP converters process the full power of attached modules or submodules, DPP subMICs only process the mismatch-related power difference between them. This allows a reduction of the power rating of DPP converters to a fraction of the peak power, thus reducing the size and cost of distributed power electronics. Opportunities are enhanced to implement DPP architectures at very high granularity, i.e. at submodule level, effectively replacing bypass diodes, or even at the cell level. Since cells operate closer to their individual MPP, energy capture in the presence of mismatches is improved. System efficiency expressions are summarized to point to the advantages of DPP architectures and the importance of the factors that affect DPP performance: mismatch power levels, submodule-level maximum power point tracking efficiency, as well as subMIC power conversion efficiency and power rating.

DPP architectures often employ voltage balancing of PV submodules in series for simple and distributed control, enabling operation of the PV system close to fine-granularity MPPT. The analysis and the experiments described in this paper demonstrate that the sensitivities of the MPP voltage with respect to irradiance, temperature and mismatch uniformity are relatively small. Even in exaggerated, worst-case examples, the experimentally verified energy yield is less than 2% below the true distributed maximum power point tracking. Differences can, in practice, be much smaller for at least two reasons: i) considering compensating effects of, for example, irradiance and temperature changes; ii) there exists an optimum control gain in the converter voltage regulation loop such that the submodules operate even closer to MPP values in the cases irradiance mismatches are the main sources of MPP variations.

DPP subMIC power limits affect mismatch mitigation more intensely in partial shading scenarios, where mismatched power (or currents) can reach almost 100% of the submodule peak power. For the scenarios considered in this paper, DPP subMICs rated between 30 and 40% of the submodule peak power allow energy production within 1% of fully rated subMICs. Another significant advantage of differential power processing is the lack of insertion loss. As a consequence, this approach can be used effectively even in systems where mismatch is relatively

small. Aging effects considered in this paper are assumed to increase the coefficient of variation of PV submodules linearly up to 10% at the end of life. Hence, mismatched power is in this case much smaller than in partial shading scenarios. It is shown that DPP converters rated at only 20% of the submodule peak power can deliver full mismatch mitigation in this case, achieving much better energy yield than module-level FPP approaches, while using power converters with lower power rating.

PV modules can be enhanced with DPP submodule integrated converters (subMICs) serving as backplane diode replacements to yield significant system efficiency improvements, while being rated at a fraction of the submodule peak power. As summarized in Table VI, considering typical 210-240 W PV models having 3 submodules rated between 70 and 80 W each, the DPP subMICs can be rated at approximately 30 W in residential PV systems affected by partial shading, and at approximately 15 W or even less in commercial or utility scale systems affected by aging and other inherent parameter dispersion.

ACKNOWLEDGMENT

The authors would like to thank Sara M. MacAlpine for providing shading data in Scenarios II and III.

REFERENCES

[1] M. C. Alonso-Garcia, J. M. Ruiz, and F. Chenlo, "Experimental study of mismatch and shading effects in the I-V characteristic of a photovoltaic module," *Solar Energy Materials and Solar Cells*, vol. 90, no. 3, pp. 329–340, 2006.

[2] C. Deline, "Partially shaded operation of multi-string photovoltaic systems," in *IEEE Photovoltaic Specialists Conference (PVSC)*, 20-25 June 2010 2010, pp. 394–399.

[3] R. Wills, S. Krauthamer, A. Bulawka, and J. Posbic, "The AC photovoltaic module concept," in *Proc. of the Intersociety Energy Conversion Engineering Conference*, vol. 3, August 1997, pp. 1562–1563.

[4] G. Walker and P. Sernia, "Cascaded DC-DC converter connection of photovoltaic modules," *IEEE Transactions on Power Electronics*, vol. 19, no. 4, pp. 1130–1139, 2004.

[5] L. Linares, R. W. Erickson, S. MacAlpine, and M. Brandemuehl, "Improved energy capture in series string photovoltaics via smart distributed power electronics," in *Proc. of the IEEE Applied Power Electronics Conference and Exposition*, 15-19 Feb. 2009, pp. 904–910.

[6] S. Poshtkouhi, A. Biswas, and O. Trescases, "DC-DC converter for high granularity, sub-string MPPT in photovoltaic applications using a virtual-parallel connection," in *Proc. of the IEEE Applied Power Electronics Conference and Exposition*, Orlando, 2012, pp. 86–92.

[7] R. C. N. Pilawa-Podgurski and D. J. Perreault, "Submodule integrated distributed maximum power point tracking for solar photovoltaic applications," *IEEE Transactions on Power Electronics*, vol. 28, no. 6, pp. 2957–2967, 2013.

[8] Y. Nimni and D. Shmilovitz, "A returned energy architecture for improved photovoltaic systems efficiency," in *Proc. of the IEEE International Symposium on Circuits and Systems*, May 30 - June 2 2010, pp. 2191–2194.

[9] P. S. Shenoy, K. A. Kim, B. B. Johnson, and P. T. Krein, "Differential power processing for increased energy production and reliability of photovoltaic systems," *IEEE Transactions on Power Electronics*, vol. 28, no. 6, pp. 2968–2979, 2013.

[10] J. T. Stauth, M. D. Seeman, and K. Kesarwani, "Resonant switched-capacitor converters for sub-module distributed photovoltaic power management," *IEEE Transactions on Power Electronics*, vol. 28, no. 3, pp. 1189–1198, 2013.

[11] C. Olalla, M. Rodriguez, D. Clement, and D. Maksimovic, "Architectures and control of submodule integrated DC-DC converters for photovoltaic applications," *IEEE Transactions on Power Electronics*, vol. 28, no. 6, pp. 2980–2997, 2012.

[12] S. MacAlpine, M. Brandemuehl, and R. Erickson, "Potential for recoverable power: Simulated use of distributed power converters at various levels in partially shaded photovoltaic arrays," in *26th European Photovoltaic Solar Energy Conference and Exhibition*, 2011.

[13] C. Olalla, C. Deline, and D. Maksimovic, "Performance of mismatched PV systems with submodule integrated converters," *IEEE Journal of Photovoltaics*, vol. 4, no. 1, pp. 396–404, 2014.

[14] K. A. Kim and P. T. Krein, "Photovoltaic hot spot analysis for cells with various reverse-bias characteristics through electrical and thermal simulation," in *Proc. of the IEEE Workshop on Control and Modeling for Power Electronics*, Salt Lake City, UT, 2013.

[15] ——, "Hot spotting and second breakdown effects on reverse I-V characteristics for mono-crystalline Si photovoltaics," in *Proc. of the IEEE Energy Conversion Congress and Exposition, ECCE'13*, Denver, CO, September 2013.

[16] S. M. MacAlpine, R. W. Erickson, and M. J. Brandemuehl, "Characterization of power optimizer potential to increase energy capture in photovoltaic systems operating under nonuniform conditions," *IEEE Transactions on Power Electronics*, vol. 28, no. 6, pp. 2936–2945, 2013.

[17] K. A. Kim, P. S. Shenoy, and P. T. Krein, "Photovoltaic differential power converter trade-offs as a consequence of panel variation," in *Proc. of the IEEE Workshop on Control and Modeling for Power Electronics*, 10-13 June 2012, pp. 1–7.

[18] S. Poshtkouhi, J. Varley, R. Popuri, and O. Trescases, "Analysis of distributed peak power tracking in photovoltaic systems," in *Proc. of the Int. Power Electronics Conf. (IPEC)*, 21-24 June 2010, pp. 942–947.

[19] S. Qin, S. T. Cady, A. D. Dominguez-Garcia, and R. C. N. Pilawa-Podgurski, "A distributed approach to MPPT for PV sub-module differential power processing," in *Proc. of the IEEE Energy Conversion Congress and Exposition, ECCE'13*, Denver, Co, September 2013.

[20] D. L. King, W. E. Boyson, and J. A. Kratochvil, "Photovoltaic array performance model," Sandia National Laboratories, Tech. Rep. SAND2004-3535, 2004.

[21] N. Blair, M. Mehos, C. Christensen, and C. Cameron, "Modeling photovoltaic and concentrating solar power through performance, cost and financing with the solar advisor model," in *Proc. of SOLAR 2008 - American Solar Energy Society*, San Diego, California, USA, 2008.

[22] Y. Levron, D. Clement, D. Maksimovic, and C. Olalla, "Nonlinear control design for the photovoltaic isolated-port architecture with submodule integrated converters," in *Proc. of the IEEE Energy Conversion Congress and Exposition, ECCE'13*, Denver, CO, September 2013.

[23] P. S. Shenoy, K. A. Kim, and P. T. Krein, "Comparative analysis of differential power conversion architectures and controls for solar photovoltaics," in *Proc. of the IEEE Workshop on Control and Modeling for Power Electronics, COMPEL'12*, June 2012, pp. 1–7.

[24] C. Deline and S. MacAlpine, "Use conditions and efficiency measurements of DC power optimizers for photovoltaic systems," in *Proc. of the IEEE Energy Conversion Congress and Exposition*, Denver, CO, 2013.

[25] C. Olalla, D. Clement, D. Maksimovic, and C. Deline, "A cell-level photovoltaic model for high-granularity simulations," in *Proc. of the IEEE European Conference on Power Electronics and Applications (EPE-ECCE)*, September 2013.

[26] C. Olalla, D. Clement, B. Seok Choi, and D. Maksimovic, "A branch and bound algorithm for high-granularity pv simulations with power limited submics," in *Proc. of the IEEE Workshop on Control and Modeling for Power Electronics, COMPEL'13*, June 2013.

[27] S. Poshtkouhi, V. Palaniappan, M. Fard, and O. Trescases, "A general approach for quantifying the benefit of distributed power electronics for fine grained MPPT in photovoltaic applications using 3-D modeling," *IEEE Transactions on Power Electronics*, vol. 27, no. 11, pp. 4656–4666, 2012.

[28] D. Jordan, J. Wohlgemuth, and S. Kurtz, "Technology and climate trends in PV module degradation," in *27th European Photovoltaic Solar Energy Conference and Exhibition, PVSEC*, Frankfurt, Germany, September 24-28 2012.